LETTER

doi:10.1038/nature12799

Mycobacteria manipulate macrophage recruitment through coordinated use of membrane lipids

C. J. Cambier[1], Kevin K. Takaki[2], Ryan P. Larson[1,3], Rafael E. Hernandez[4], David M. Tobin[2], Kevin B. Urdahl[1,3,4], Christine L. Cosma[2] & Lalita Ramakrishnan[1,2,5]

The evolutionary survival of *Mycobacterium tuberculosis*, the cause of human tuberculosis, depends on its ability to invade the host, replicate, and transmit infection. At its initial peripheral infection site in the distal lung airways, *M. tuberculosis* infects macrophages, which transport it to deeper tissues[1]. How mycobacteria survive in these broadly microbicidal cells is an important question. Here we show in mice and zebrafish that *M. tuberculosis*, and its close pathogenic relative *Mycobacterium marinum*, preferentially recruit and infect permissive macrophages while evading microbicidal ones. This immune evasion is accomplished by using cell-surface-associated phthiocerol dimycoceroserate (PDIM) lipids[2] to mask underlying pathogen-associated molecular patterns (PAMPs). In the absence of PDIM, these PAMPs signal a Toll-like receptor (TLR)-dependent recruitment of macrophages that produce microbicidal reactive nitrogen species. Concordantly, the related phenolic glycolipids (PGLs)[2] promote the recruitment of permissive macrophages through a host chemokine receptor 2 (CCR2)-mediated pathway. Thus, we have identified coordinated roles for PDIM, known to be essential for mycobacterial virulence[3], and PGL, which (along with CCR2) is known to be associated with human tuberculosis[4,5]. Our findings also suggest an explanation for the longstanding observation that *M. tuberculosis* initiates infection in the relatively sterile environment of the lower respiratory tract, rather than in the upper respiratory tract, where resident microflora and inhaled environmental microbes may continually recruit microbicidal macrophages through TLR-dependent signalling.

Pattern recognition receptors (PRRs) such as the TLRs enable host recognition of diverse microbes through their PAMPs[6]. Macrophages recruited through TLR signalling pathways can eradicate organisms invading the oropharyngeal mucosa, for example, *Streptococcus pneumoniae*[7]. In contrast, pathogenic mycobacteria appear to use macrophages and myeloid dendritic cells for transport across epithelial barriers to their infection niche[1,8]. Mycobacteria are replete with TLR PAMPs—such as lipoproteins and bacterial cell wall peptidoglycan—that have been shown to activate cytokine responses in cultured macrophages[1]. Yet *in vivo* studies find TLR signalling to be dispensable in the early stages of infection[9], suggesting that mycobacteria have evolved mechanisms to circumvent the bactericidal consequences of TLR signalling.

To explore these mechanisms, we used zebrafish larvae infected with *M. marinum*, a close genetic relative of *M. tuberculosis* and the causative agent of tuberculosis in ectotherms. This model has yielded important insights into the pathogenesis and genetics of human tuberculosis[10]. In humans, the earliest interactions between mycobacteria and phagocytes occur at the lung epithelial surface. Such interactions can be modelled in the larva by injection of bacteria or other chemical stimuli into the hindbrain ventricle (HBV), a neuroepithelium-lined cavity to which phagocytes are recruited[8] (Fig. 1a). We used morpholino knockdown to create zebrafish deficient in MyD88, a common downstream adaptor molecule for TLR signalling pathways[6]. As expected, MyD88 morphants had decreased macrophage recruitment to *Staphylococcus aureus* and *Pseudomonas aeruginosa*, mucosal bacteria that can be commensal or pathogenic[11–13] (Fig. 1b). Similarly, macrophage recruitment to the nonpathogenic *Mycobacterium smegmatis* was MyD88 dependent. In contrast, macrophage recruitment to *M. marinum* was MyD88 independent (Fig. 1c). This finding suggested that pathogenic mycobacteria have the ability to mask PAMPs that would otherwise induce TLR signalling during the initial infection phase. We proposed that such a factor would be a cell-surface-associated virulence determinant. In this light, PDIM seemed a likely candidate, particularly because it is present only in pathogenic mycobacteria, including *M. tuberculosis* and *M. marinum*, but absent in non-pathogenic *M. smegmatis*[2]. We created a *M. marinum* mutant that lacks PDIM on its surface by knocking out the PDIM transporter, encoded by the *mmpL7* gene, and confirmed that it was attenuated in zebrafish larvae (Fig. 1d and Extended Data Fig. 2). If PDIM is masking PAMPs, then macrophage recruitment to Δ*mmpL7* bacteria should be MyD88 dependent, and this was the case (Fig. 1e). In contrast, macrophage migration remained MyD88 independent in response to *M. marinum* deficient in another cell-surface-associated virulence determinant, Erp (Δ*erp*) (Fig. 1d, e and Extended Data Fig. 2)[14]. This result was consistent with *M. smegmatis* possessing a functional *erp*[14], and suggested further that the evasion of MyD88-dependent immune detection was mediated specifically by PDIM.

Our model posits that pathogenic mycobacteria use PDIM to evade recruitment of MyD88-dependent macrophage populations detrimental to their survival. Therefore, we predicted that wild-type mycobacteria would be unaffected in MyD88 morphants, whereas the attenuation of Δ*mmpL7* should be reversed. We found both to be the case (Fig. 1f). For these assays, approximately 80 *M. marinum* were injected into the HBV. However, MyD88 morphants were previously reported to be susceptible to higher *M. marinum* inocula delivered intravenously[15]. We confirmed these findings, showing that MyD88 deficiency increased susceptibility at later time points after intravenous administration of >300 colony forming units (c.f.u.) (Extended Data Fig. 3). It is likely that MyD88 exerts its protective responses at these later stages through mechanisms distinct from the ones we have uncovered, such as through interleukin (IL)-1-mediated responses[9]. Indeed, IL-1 expression was undetectable 3 h after infection, when we observed MyD88-dependent macrophage recruitment (data not shown), suggesting an IL-1-independent role for MyD88 in mediating recruitment towards PDIM-deficient mycobacteria.

Further characterization of wild-type versus PDIM-deficient bacteria revealed that both strains recruited cells expressing the macrophage-specific marker Mpeg1 (ref. 8) (Extended Data Fig. 4a and Supplementary Videos 1, 2). We next asked whether these macrophages possessed differential microbicidal potential. We examined the expression of inducible nitric oxide synthase (iNOS) in these recruited cells because: (1) it is induced in macrophages upon TLR signalling[6], and can be expressed by zebrafish[16], mouse[17] and human[18] macrophages after mycobacterial infection; and (2) mycobacteria are known to be susceptible to reactive

[1]Department of Immunology, University of Washington, Seattle, Washington 98195, USA. [2]Department of Microbiology, University of Washington, Seattle, Washington 98195, USA. [3]Seattle Biomedical Research Institute, Seattle, Washington 98109, USA. [4]Department of Pediatrics, University of Washington, Seattle, Washington 98195, USA. [5]Department of Medicine, University of Washington, Seattle, Washington 98195, USA.

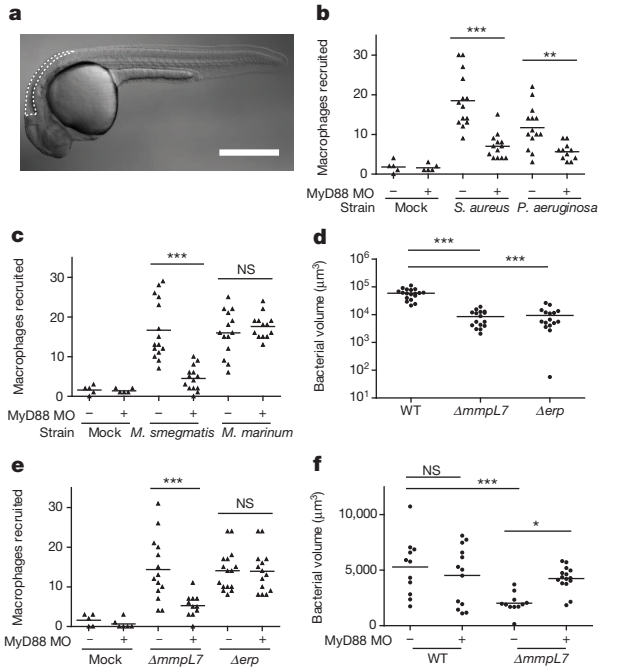

Figure 1 | PDIM-mediated evasion of MyD88-dependent macrophage recruitment. a, Schematic of a 2 days post-fertilization (dpf) zebrafish showing the HBV injection site outlined with dashed white line. Scale bar, 500 μm. **b**, **c**, Mean macrophage recruitment at 3 h post-infection (hpi) into the HBV of wild-type or MyD88-morphant (MO) fish after infection with 150 *S. aureus*, 200 *P. aeruginosa* (**b**), 80 *M. marinum* or 85 *M. smegmatis* (**c**). Representative of three separate experiments. **d**, Mean bacterial burdens at 3 dpi after HBV infection of wild-type (WT) fish with 80 wild-type, Δ*mmpL7* or Δ*erp* *M.marinum*. Representative of three separate experiments. **e**, Mean macrophage recruitment at 3 hpi into the HBV of wild-type or MyD88-morphant fish after infection with Δ*mmpL7* or Δ*erp* *M. marinum*. Representative of four separate experiments. **f**, Mean bacterial burdens of wild-type or MyD88-morphant fish at 3 dpi after HBV infection with wild-type or Δ*mmpL7* *M. marinum*. Representative of three separate experiments. Significance testing for all panels done using one-way analysis of variance (ANOVA), with Bonferroni's post-test for comparisons shown. $*P < 0.05$, $***P < 0.001$. NS, not significant.

nitrogen species (RNS) in both murine[17] and human[18] macrophages. We found very few iNOS-positive macrophages arriving in response to wild-type *M. marinum*, whereas the majority of those arriving in response to Δ*mmpL7* bacteria were iNOS positive (Fig. 2a–c and Extended Data Fig. 4b). Δ*erp* bacteria elicited very few iNOS-expressing macrophages (Fig. 2c and Extended Data Fig. 4b), further showing that this early manipulation of macrophage recruitment and/or activation is a specific characteristic of PDIM. We confirmed that RNS were the major mediators of MyD88-dependent macrophage microbicidal activity by showing that the nitric oxide scavenger carboxy-2-phenyl-4,4,5,5-tetramethylimidazolinone-3-oxide-1-oxyl (CPTIO) and N^G-nitro-L-arginine methyl ester hydro-chloride (L-NAME) reversed growth attenuation of the Δ*mmpL7* mutant (Fig. 2d and Extended Data Fig. 4c).

Together, our findings suggested that PDIM mediates an immune evasion strategy, whereby mycobacteria evade detection by TLRs so as to avoid recruitment of iNOS-expressing, microbicidal macrophages. To test this idea, we co-infected red fluorescent wild-type bacteria with green fluorescent wild-type or Δ*mmpL7* bacteria. We found that wild-type bacteria were attenuated in the presence of Δ*mmpL7* bacteria, and that this attenuation transfer was specifically caused by co-infection with Δ*mmpL7* and not with wild-type or Δ*erp* bacteria (Fig. 2e and Extended Data Fig. 5a, b). Furthermore, this transfer of attenuation from Δ*mmpL7* to wild-type bacteria was dependent on macrophages; no attenuation was observed when macrophages were depleted before infection using a morpholino against the myeloid transcription factor PU.1 (Fig. 2f)[16]. Attenuation transfer was similarly dependent on MyD88 signalling, as well as on RNS production (Fig. 2g, h and Extended Data Fig. 5c).

As PDIM is not the only substrate for the MmpL7 transporter, we confirmed that the effects we observed were due to the lack of PDIM *per se* by using a PDIM synthesis mutant, Δ*mas*, showing it to both recruit macrophages in a MyD88-dependent fashion and to transfer attenuation to wild-type bacteria (Extended Data Fig. 6). Finally, to rule out the possibility that the PDIM-deficient mutants simply had increased expression of the culpable PAMP(s), we co-injected heat-killed, crushed wild-type bacteria together with live wild-type bacteria. If the culpable PAMP(s) are expressed by wild-type bacteria, then these PAMPs should become exposed by crushing the bacteria and cause attenuation of the live bacteria. We found this to be the case (Fig. 2i). Altogether, these results suggest that PDIM physically masks underlying mycobacterial PAMPs, thereby preventing mycobacterial delivery into microbicidal macrophages.

To corroborate our findings in a second model, we infected mice through the aerosol route with wild-type *M. tuberculosis* (H37Rv) or with an isogenic strain (Δ*drrA*) defective for proper PDIM surface localization and virulence in mice[3]. At 21 days post-infection (dpi), we found substantially greater proportions of iNOS-producing cells among the $CD11b^+Ly6C^{hi}$ inflammatory monocyte population in the lungs of mice infected with the Δ*drrA* mutant compared to mice infected with the wild-type strain (Fig. 3 and Extended Data Fig. 7). Thus, PDIM-mediated evasion of TLR-dependent immune recognition is shared by *M. tuberculosis* in the context of the mammalian lung, consistent with its central role in avoidance of TLR-dependent antimicrobial mechanisms such as iNOS and antimicrobial peptides[6].

We next sought to understand the mechanism by which mycobacteria recruit the permissive macrophages that are essential for their transport into host tissues. Given our previous finding that *M. marinum* recruits only macrophages (and not neutrophils) to the HBV[8], we considered macrophage-specific chemokines as candidates for mediating this recruitment. We investigated CCR2, which has been implicated in macrophage migration to bacterial pathogens in mice[19], including macrophages that are permissive to *M. tuberculosis* replication after aerosol infection[20]. We identified the functional zebrafish CCR2 orthologue (see Methods) and confirmed that its knockdown resulted in reduced macrophage migration in response to recombinant human chemokine ligand 2 (CCL2) and not to the closely related human macrophage chemokines CCL4 and CCL5 (Extended Data Fig. 8a). The specificity of CCL2-mediated macrophage migration was revealed by the following findings: (1) human and mouse CCL2 induced macrophage but not neutrophil migration (Extended Data Fig. 8b, c); (2) recombinant human IL-8, a neutrophil chemokine, induced neutrophil but not macrophage migration (Extended Data Fig. 8b, c); (3) human leukotriene B4 (LTB4) induced recruitment of both neutrophils and macrophages (Extended Data Fig. 8b, c), as expected[16]; and (4) MyD88 knockdown did not diminish CCL2-mediated macrophage migration, ruling out TLR-mediated migration in response to any endotoxin that might be contaminating the chemokine preparations (Extended Data Fig. 8b).

CCR2 morphants had reduced macrophage migration in response to wild-type *M. marinum*, confirming the role of this pathway in recruitment (Fig. 4a). Recruitment to PDIM-deficient *M. marinum* was unaffected, showing that TLR PAMPs trigger recruitment through a CCR2-independent pathway (Fig. 4a). Accordingly, we found that *M. marinum* infection induced CCL2, and that CCL2 morphants also had reduced macrophage recruitment in response to infection (Fig. 4b and Extended Data Fig. 9).

Turning to the question of which bacterial determinant induced the CCR2 pathway, we considered PGL, a molecule closely related to PDIM in both *M. marinum* and *M. tuberculosis*[2]. Although many clinical *M. tuberculosis* isolates have lost PGL, its presence has been linked to increased virulence[5]. Moreover, among *M. tuberculosis* clinical isolates, PGL expression was linked to *Ccl2* expression in a mouse lung infection model[21]. Similarly, we found that PGL was required for *ccl2* induction in the zebrafish larva; deletion of the *M. marinum pks15* locus

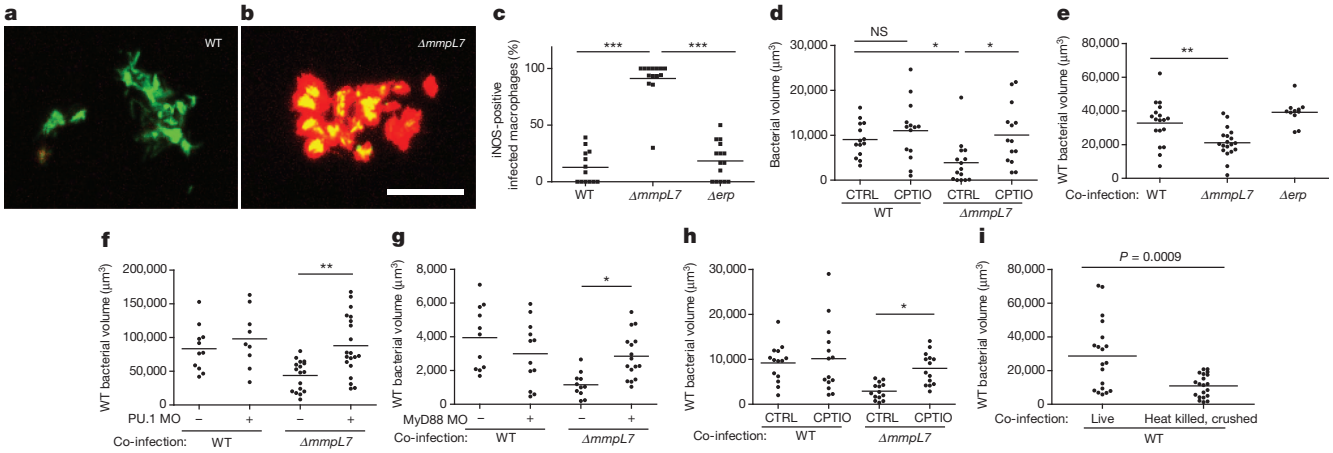

Figure 2 | Increased iNOS-dependent microbicidal activity of macrophages recruited to PDIM-deficient mycobacteria. **a**, **b**, Representative images of wild-type (WT) (**a**) and Δ*mmpL7* (**b**) *M. marinum*-infected fish from **c**. $N = 13$ (wild-type) and 14 (Δ*mmpL7*) larvae per group. Scale bar, 50 μm. **c**, Percentage of infected macrophages that were iNOS positive in the HBV at 3 dpi with 80 wild-type, Δ*mmpL7* or Δ*erp M. marinum*. Representative of three separate experiments. **d**, Mean bacterial burdens of 2 dpf control (CTRL)- or RNS scavenger (CPTIO)-treated fish after HBV infection with 80 wild-type or Δ*mmpL7 M. marinum*. Representative of two separate experiments. NS, not significant. **e**–**h**, Mean bacterial volume of red fluorescent wild-type *M. marinum* (infection inoculum 30–40) when co-infected with 30–40 green fluorescent wild-type, Δ*mmpL7* or Δ*erp M. marinum* at 3 dpi in wild-type (**e**), PU.1-morphant (MO) (**f**), MyD88-morphant (**g**), or CPTIO-treated (**h**) larvae. **e**, **g**, Co-infection of wild-type and Δ*mmpL7 M. marinum* in wild-type or MyD88-morphant fish is representative of at least three separate experiments, and co-infection with Δ*erp* is representative of two separate experiments. **f**, **h**, Representative of two separate experiments. **a**–**h**, Significance testing done using one-way ANOVA, with Bonferroni's post-test for comparisons shown. $*P < 0.05$, $**P < 0.01$, $***P < 0.001$. **i**, Mean bacterial volume of red fluorescent wild-type *M. marinum* at 3 dpi (infecting inoculum 30–40) when co-infected with the volume equivalent of 30–40 heat-killed, crushed wild-type *M. marinum*. Representative of two separate experiments. Student's unpaired *t*-test.

specifically abrogates PGL, but not PDIM, production (data not shown) and resulted in loss of *ccl2* induction. Δ*mmpL7* bacteria, which lack surface expression of both PGL and PDIM, similarly failed to induce *ccl2*, highlighting that this chemokine is not induced through TLR interactions, but rather is specifically induced through PGL-mediated interactions (Fig. 4b). Furthermore, Δ*pks15* bacteria recruited fewer macrophages upon infection of wild-type larvae, and this reduction was similar to that seen in CCR2 morphants infected with wild-type bacteria (Fig. 4c). There was no additional reduction in recruitment when CCR2 morphants were infected with PGL-deficient bacteria, suggesting that PGL recruits macrophages solely through the CCR2 pathway (Fig. 4c).

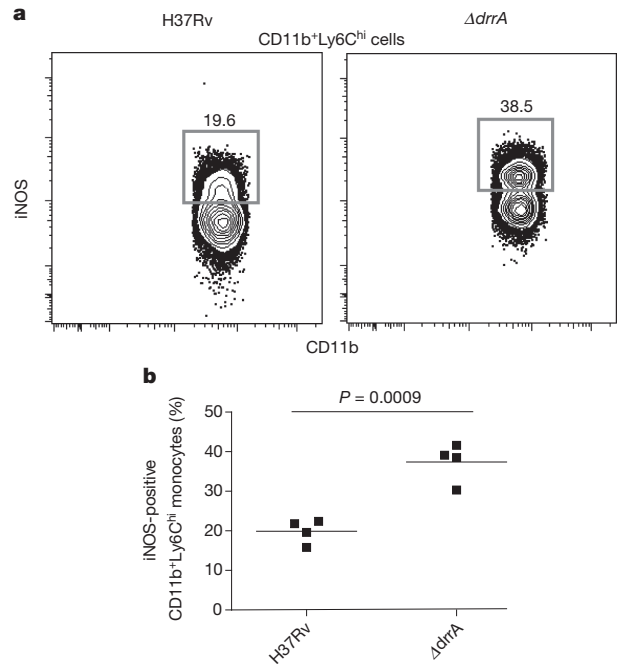

Figure 3 | Elevated frequencies of iNOS-expressing inflammatory monocytes in mice infected with PDIM-deficient *M. tuberculosis*. **a**, **b**, C57BL/6 mice were infected through the aerosol route with H37Rv or an isogenic PDIM-deficient mutant (Δ*drrA*). Lung tissue was harvested at 21 dpi and iNOS protein expression was measured using flow cytometry. Representative fluorescence-activated cell sorting (FACS) plots (**a**) and graphical depiction (**b**) of frequencies of iNOS-expressing cells within the $CD11b^+Ly6C^{hi}$ inflammatory monocyte population. Representative of two separate experiments. Student's unpaired *t*-test.

Our findings implicate PGL in bacterial virulence and, correspondingly, the CCR2 pathway in host susceptibility. Globally, a large proportion of *M. tuberculosis* isolates are PGL deficient due to a frameshift in *pks15* (ref. 2). However, the importance of PGL in mediating virulence and/or transmission is underscored by its presence in many of the W-Beijing strains, which are becoming rapidly enriched among *M. tuberculosis* isolates globally[5], and have predominated in outbreaks in North America, where tuberculosis is not prevalent[5]. Infectivity is a key requirement for transmission, and our data suggested that PGL may enhance infectivity through CCR2-mediated recruitment of permissive macrophages at the earliest stages of infection. This enhancement may be particularly relevant in the context of human infections, in which the infectious dose is thought to be as low as 1–3 bacteria[22,23]. To test the hypothesis that PGL enhances infectivity at low doses, we compared the ability of wild-type and PGL-deficient strains to establish infection. Confocal microscopy was used 5 hours after HBV injection to select those animals that had received 1–3 bacteria (Extended Data Fig. 10), and then again at 5 dpi to identify which animals were still infected. We found that 89% of the wild-type but only 18% of the Δ*pks15* infections were successful (Fig. 4d). Concurrent administration of recombinant CCL2 restored the infectivity of Δ*pks15* bacteria, provided the CCR2 pathway was intact (Fig. 4d). Correspondingly, we found that wild-type bacteria had a lower infectivity rate in CCR2 morphants (Fig. 4d). Consistent with our finding that PGL recruits macrophages solely through CCR2, there was no further decrease in infectivity in CCR2 morphants infected with the PGL mutant (Fig. 4d). Finally, the infectivity of wild-type bacteria in MyD88 morphants was undiminished (90% for wild type versus 83% for morphants), consistent with our finding that TLR signalling is not involved in macrophage recruitment to wild-type bacteria.

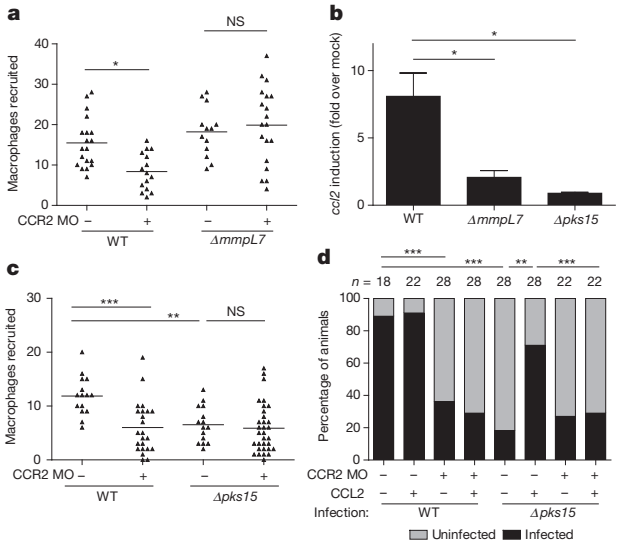

Figure 4 | Macrophage recruitment and subsequent infectivity is mediated by mycobacterial PGL and host CCR2. **a**, Mean macrophage recruitment at 3 hpi into the HBV of wild-type or CCR2-morphant (MO) fish after infection with 80 wild-type (WT) or Δ*mmpL7 M. marinum*. Representative of three independent experiments. One-way ANOVA, with Bonferroni's post-test for comparisons shown. $*P < 0.05$. **b**, *ccl2* messenger RNA levels (mean ± standard error of the mean (s.e.m.) of four biological replicates) induced at 3 h after caudal vein infection of 2 dpf larvae with 250–300 wild-type, Δ*pks15* or Δ*mmpL7 M. marinum*. One-way ANOVA with Tukey's post-test. $*P < 0.05$. **c**, Mean macrophage recruitment at 3 hpi into the HBV after infection with 80 wild-type or Δ*pks15 M. marinum*. Representative of three separate experiments. One-way ANOVA with Bonferroni's post-test for comparisons shown. $**P < 0.01$, $***P < 0.001$. **d**, Wild-type and CCR2-morphant fish, with or without the addition of 5 μg ml^{-1} CCL2, were infected in the HBV with 1–3 wild-type or Δ*pks15 M. marinum*. Graph shows the percentage of fish that were infected (black) or uninfected (grey) after 5 days. *n* = number of larvae per group. Representative of two separate experiments. Significance was evaluated using Fisher's exact test for each comparison. $**P < 0.01$, $***P < 0.001$. NS, not significant.

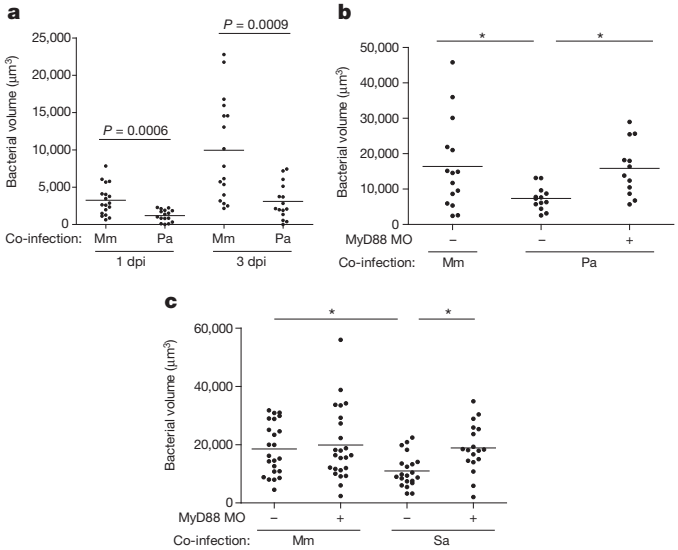

Figure 5 | MyD88-dependent macrophage recruitment elicited by other bacterial pathogens and commensals attenuates pathogenic mycobacteria. **a**, Mean bacterial volume of red fluorescent *M. marinum* (infecting inoculum 30–40) after co-infection with either 30–40 green fluorescent *M. marinum* (Mm) or 300 *P. aeruginosa* (Pa) at 1 and 3 dpi. Representative of three separate experiments. Significance assessed using Student's *t*-test. **b**, **c**, Mean bacterial volume of 30–40 red fluorescent wild-type *M. marinum* (infecting inoculum 30–40) after co-infection with either 30–40 green fluorescent wild-type *M. marinum* or 300 *P. aeruginosa* (**b**) or 300 *S. aureus* (Sa) (**c**) at 3 dpi, in wild-type or MyD88-morphant (MO) larvae. Significance tested by one-way ANOVA with Bonferroni's post-test for comparisons shown. $*P < 0.05$.

These findings highlight the interdependency between bacterial PGL and host CCR2 signalling in driving bacterial infectivity under the low inoculum conditions relevant to human infection. Previous investigations into the role of PGL and CCR2 may have failed to reveal these mechanisms because those studies used higher inocula[24] and, in the study of CCR2 signalling, a PGL-deficient strain[25]. Indeed, our finding that CCR2 signalling is a host susceptibility factor is reinforced by human studies showing an association between the high expression of CCL2 and tuberculosis susceptibility[4]. Furthermore, the association appears to be stronger in east Asian populations[26], where clinical isolates are enriched for the predominantly PGL-expressing W-Beijing strains[27]. In light of our findings, we propose that the enrichment of PGL expression among these strains is influencing this association, as the CCR2 pathway would be most relevant in the context of bacterial PGL stimulation.

Finally, our data suggested an explanation for why *M. tuberculosis* must reach the alveolar surfaces of the distal lung in order to initiate infection[23] (Extended Data Fig. 1). It is well established that tuberculosis results from inhalation of small aerosol droplets containing ~1–3 bacteria, which are capable of reaching the alveolar surfaces of the distal lung; in contrast, large droplets harbouring ~10^4 bacteria are trapped in the upper bronchial passages and are far less successful at establishing infection[22,23]. These observations have led to the idea that the alveolar surfaces of the distal lung offer a more favourable environment for mycobacterial proliferation. We wondered if commensal microbes from the oropharyngeal surfaces, as well as inhaled environmental organisms, might lead to continual TLR signalling in the upper respiratory tract that would then override the mycobacterial PDIM-dependent immune evasion strategies we identified. In contrast, the lower respiratory tract, which is relatively sterile[28], would favour recruitment of *Mycobacterium*-permissive macrophages. To test this hypothesis, we co-infected animals with *M. marinum* together with bacterial colonizers of the pharynx that induce TLR signalling—either *S. aureus*, a common Gram-positive colonizer of the nasopharynx in both adults and children[12], or the Gram-negative bacterium *P. aeruginosa,* also reported to colonize the pharynx of asymptomatic adults and children[11]. Co-infection with *P. aeruginosa* resulted in the attenuation of wild-type mycobacteria by 1 dpi, and continued into 3 dpi (Fig. 5a). Mycobacterial growth was attenuated despite rapid clearing of *P. aeruginosa*: 56% of the animals had cleared the co-infected *P. aeruginosa* by 1 dpi, and 76% by 3 dpi, with only a few residual bacteria in the remaining animals. Thus, it was not the physical presence of, but rather the detrimental immunological milieu induced by *P. aeruginosa* that was responsible for the attenuation of *M. marinum*. Consistent with our hypothesis, we found that the detrimental effect of *P. aeruginosa* on mycobacterial survival was MyD88 dependent (Fig. 5b). *S. aureus* co-infection also had a MyD88-dependent detrimental effect on *M. marinum* survival (Fig. 5c).

Our previous work identified strategies by which intracellular mycobacteria manipulate host pathways after having traversed epithelial barriers; these involve a bacterial protein secretion system that expands the bacterial niche through macrophage recruitment to the nascent granuloma[10]. We now describe what may be the first contact between mycobacteria and their hosts, and the manner in which mycobacteria manipulate recruitment, and potentially influence the differentiation or activation state of the first responding macrophages so as to gain access to their preferred niche (Extended Data Fig. 1). The choreographed entry involves two related mycobacterial lipids acting in concert to avoid one host pathway while inducing another. Our findings link PDIM, recognized as an absolutely essential mycobacterial virulence factor, to the evasion of TLR detection and thus explain the dispensability of TLR-mediated immunity in protection against *M. tuberculosis* infection in both human and animal studies[9,29]. In contrast, PGL is dispensable for virulence, being variably present among clinical isolates. Yet its presence in the ancestral *M. cannetti* strains as well as in *M. marinum*,

the closest genetic relative of the *M. tuberculosis* complex[2], suggests its integral role in the evolution of mycobacterial pathogenicity. Tuberculosis is an ancient disease, and the enhanced infectivity conferred by PGL may have been essential for most of its history before human crowding, with its greatly increased opportunities for transmission, made it dispensable[30].

Our findings suggest a central role for commensal flora in choreographing mycobacterial entry. Not only must pathogenic mycobacteria possess a physical barrier to prevent host TLR-mediated detection, but they must also evade TLR signalling initiated by other organisms, by entering through the distal lung (Extended Data Fig. 1). Our work may also explain the paradox that smaller *M. tuberculosis* droplets are more infectious than larger ones. However, the requirement placed on mycobacteria to gain entry through the distal lung makes tuberculosis less contagious than most other respiratory infections, thus assigning a protective role to the commensal flora. Conversely, the persistence of human tuberculosis for over 70,000 years[30] attests to the effectiveness of the mycobacterial evolutionary survival kit (masking lipid, recruiting lipid and small infection droplets) to simultaneously evade and manipulate the host and its commensal flora.

METHODS SUMMARY

M. marinum, *S. aureus* and *P. aeruginosa* constitutively expressed fluorescent proteins GFP, Wasabi or tdTomato to allow visualization. Zebrafish larvae (of undetermined sex given the early developmental stages used) were infected at 36–48 h post-fertilization (hpf) via caudal vein or HBV injection. Larvae were randomly allotted to the different experimental conditions. Fluorescence images were captured and quantitative fluorescence was used as a surrogate for bacterial burdens. For the macrophage recruitment assays, macrophages and neutrophils in the HBV were enumerated using differential interference contrast microscopy 3 h after HBV infection. For determination of infection burdens in the HBV, 1 and 3 dpi larvae were mounted in 1.5% agarose (low melting point) and confocal z-stacks of 2 μm were obtained. For the infectivity assay, 2 dpf larvae were injected in the HBV with a concentration of mycobacteria that resulted in an average of 0.8 bacteria per injection. Larvae harbouring 1–3 bacteria were identified at 5 hpi using confocal microscopy, and were re-imaged at 5 dpi and scored as infected or uninfected. Antibody staining for iNOS was performed as described[8] by confocal microscopy. CPTIO (Sigma) was used at a final concentration of 500 μM in 0.1% dimethylsulphoxide in fish water. Larvae were incubated immediately after infection and fresh CPTIO was added every 24 h for the duration of the experiment. For quantitative real-time PCR, complementary DNA was synthesized from pools of 20–40 larvae as previously described[8]. *ccl2* RNA levels were determined using SYBR green and the primers 5′-GTCTGGTGCTCTTCGCTTTC-3′ and 5′-TGCAGAG AAGATGCGTCGTA-3′. Ten-week-old female C57BL/6 mice were infected through the aerosol route with *M. tuberculosis* strains. For iNOS staining, lungs were harvested and processed at 21 dpi. Statistical analyses were formed using Graphpad Prism software. Zebrafish and mouse husbandry and all experiments performed on them were in compliance with Institutional Animal Care and Use Committee approved protocols.

Online Content Any additional Methods, Extended Data display items and Source Data are available in the online version of the paper; references unique to these sections appear only in the online paper.

Received 21 May; accepted 18 October 2013.
Published online 15 December 2013.

1. Philips, J. A. & Ernst, J. D. Tuberculosis pathogenesis and immunity. *Annu. Rev. Pathol.* **7,** 353–384 (2012).
2. Onwueme, K. C., Vos, C. J., Zurita, J., Ferreras, J. A. & Quadri, L. E. N. The dimycocerosate ester polyketide virulence factors of mycobacteria. *Prog. Lipid Res.* **44,** 259–302 (2005).
3. Murry, J. P., Pandey, A. K., Sassetti, C. M. & Rubin, E. J. Phthiocerol dimycocerosate transport is required for resisting interferon-γ-independent immunity. *J. Infect. Dis.* **200,** 774–782 (2009).
4. Flores-Villanueva, P. O. *et al.* A functional promoter polymorphism in monocyte chemoattractant protein-1 is associated with increased susceptibility to pulmonary tuberculosis. *J. Exp. Med.* **202,** 1649–1658 (2005).
5. Reed, M. B. *et al.* A glycolipid of hypervirulent tuberculosis strains that inhibits the innate immune response. *Nature* **431,** 84–87 (2004).
6. Medzhitov, R. Recognition of microorganisms and activation of the immune response. *Nature* **449,** 819–826 (2007).
7. Weiser, J. N. The pneumococcus: why a commensal misbehaves. *J. Mol. Med.* **88,** 97–102 (2010).
8. Yang, C.-T. *et al.* Neutrophils exert protection in the early tuberculous granuloma by oxidative killing of mycobacteria phagocytosed from infected macrophages. *Cell Host Microbe* **12,** 301–312 (2012).
9. Mayer-Barber, K. D. *et al.* Cutting edge: caspase-1 independent IL-1 production is critical for host resistance to *Mycobacterium tuberculosis* and does not require TLR signaling *in vivo*. *J. Immunol.* **184,** 3326–3330 (2010).
10. Ramakrishnan, L. Revisiting the role of the granuloma in tuberculosis. *Nature Rev. Immunol.* **12,** 352–366 (2012).
11. Rosenthal, S. & Tager, I. B. Prevalence of Gram-negative rods in the normal pharyngeal flora. *Ann. Intern. Med.* **83,** 355–357 (1975).
12. Wertheim, H. F. L. *et al.* The role of nasal carriage in *Staphylococcus aureus* infections. *Lancet Infect. Dis.* **5,** 751–762 (2005).
13. Eddens, T. & Kolls, J. K. Host defenses against bacterial lower respiratory tract infection. *Curr. Opin. Immunol.* **24,** 424–430 (2012).
14. de Mendonça-Lima, L. *et al.* The allele encoding the mycobacterial Erp protein affects lung disease in mice. *Cell. Microbiol.* **5,** 65–73 (2003).
15. van der Vaart, M., van Soest, J. J., Spaink, H. P. & Meijer, A. H. Functional analysis of a zebrafish *myd88* mutant identifies key transcriptional components of the innate immune system. *Dis. Model. Mech.* **6,** 841–854 (2013).
16. Tobin, D. M. *et al.* The *lta4h* locus modulates susceptibility to mycobacterial infection in zebrafish and humans. *Cell* **140,** 717–730 (2010).
17. Chan, J., Xing, Y., Magliozzo, R. S. & Bloom, B. R. Killing of virulent *Mycobacterium tuberculosis* by reactive nitrogen intermediates produced by activated murine macrophages. *J. Exp. Med.* **175,** 1111–1122 (1992).
18. Kröncke, K. D., Fehsel, K. & Kolb-Bachofen, V. Inducible nitric oxide synthase in human diseases. *Clin. Exp. Immunol.* **113,** 147–156 (1998).
19. Serbina, N. V., Jia, T., Hohl, T. M. & Pamer, E. G. Monocyte-mediated defense against microbialpathogens. *Annu. Rev. Immunol.* **26,** 421–452 (2008).
20. Antonelli, L. R. V. *et al.* Intranasal Poly-IC treatment exacerbates tuberculosis in mice through the pulmonary recruitment of a pathogen-permissive monocyte/macrophage population. *J. Clin. Invest.* **120,** 1674–1682 (2010).
21. Ordway, D. *et al.* The hypervirulent *Mycobacterium tuberculosis* strain HN878 induces a potent TH1 response followed by rapid down-regulation. *J. Immunol.* **179,** 522–531 (2007).
22. Bates, J. H., Potts, W. E. & Lewis, M. Epidemiology of primary tuberculosis in an industrial school. *N. Engl. J. Med.* **272,** 714–717 (1965).
23. Wells, W. F., Ratcliffe, H. L. & Grumb, C. On the mechanics of droplet nuclei infection; quantitative experimental air-borne tuberculosis in rabbits. *Am. J. Hyg.* **47,** 11–28 (1948).
24. Sinsimer, D. *et al.* The phenolic glycolipid of *Mycobacterium tuberculosis* differentially modulates the early host cytokine response but does not in itself confer hypervirulence. *Infect. Immun.* **76,** 3027–3036 (2008).
25. Scott, H. M. & Flynn, J. L. *Mycobacterium tuberculosis* in chemokine receptor 2-deficient mice: influence of dose on disease progression. *Infect. Immun.* **70,** 5946–5954 (2002).
26. Feng, W. X. *et al.* CCL2−2518 (A/G) polymorphisms and tuberculosis susceptibility: a meta-analysis. *Int. J. Tuberc. Lung Dis.* **16,** 150–156 (2012).
27. Gagneux, S. Variable host-pathogen compatibility in *Mycobacterium tuberculosis*. *Proc. Natl Acad. Sci. USA* **103,** 2869–2873 (2006).
28. Charlson, E. S. *et al.* Topographical continuity of bacterial populations in the healthy human respiratory tract. *Am. J. Respir. Crit. Care Med.* **184,** 957–963 (2011).
29. von Bernuth, H., Picard, C., Puel, A. & Casanova, J.-L. Experimental and natural infections in MyD88- and IRAK-4-deficient mice and humans. *Eur. J. Immunol.* **42,** 3126–3135 (2012).
30. Comas, I. *et al.* Out-of-Africa migration and Neolithic coexpansion of *Mycobacterium tuberculosis* with modern humans. *Nature Genet.* **45,** 1176–1182 (2013).

Supplementary Information is available in the online version of the paper.

Acknowledgements We thank S. Falkow and P. Edelstein for sharing their knowledge and insights, P. Donald for discussions about human infectivity in tuberculosis, B. Cormack for manuscript review and editing, J. Bubeck-Wardenberg for the fluorescent *S. aureus* strain, K. Hicks for initial MyD88 experiments, T.-Y. Chen, B. Moody, P. Manzanillo and J. Cox for help with lipid analyses, and J. Cameron for fish facility management. Supported by a National Science Foundation predoctoral fellowship to C.J.C., a Senior Research Training Fellowship from the American Lung Association and the National Institutes of Health (NIH) Training Grant "Training Clinical and Basic Immunologists" to R.P.L., a NIH "Academic Pediatric Infectious Disease" Training Grant award to R.E.H., an American Cancer Society Postdoctoral Fellowship and NIH Bacterial Pathogenesis Training Grant Award to D.M.T., and NIH grants to K.B.U. and L.R. D.M.T. is a recipient of the NIH Director's New Innovator Award and L.R. is a recipient of the NIH Director's Pioneer Award.

Author Contributions C.J.C., C.L.C., K.K.T., D.M.T., R.E.H. and L.R. conceived and designed *M. marinum*/zebrafish experiments and analysed data; C.J.C., C.L.C., K.K.T., D.M.T. and R.E.H. performed these experiments; R.P.L. and K.B.U. designed the *M. tuberculosis*/mouse experiments and analysed the data; R.P.L. performed the mouse experiments; C.J.C., C.L.C. and L.R. wrote the paper; C.J.C., R.P.L. and K.K.T. prepared the figures; and all authors edited the paper.

Author Information Reprints and permissions information is available at www.nature.com/reprints. The authors declare no competing financial interests. Readers are welcome to comment on the online version of the paper. Correspondence and requests for materials should be addressed to L.R. (lalitar@uw.edu).

METHODS

Bacterial strains and methods. *M. marinum* strain M (ATCC BAA-535) and the Δ*erp* mutant have been described[31]. The Δ*mmpL7* and Δ*pks15* mutants were generated as described in the following section. Fluorescently labelled bacterial strains were generated by transformation with the pTEC15 or pTEC27 plasmids (deposited with Addgene, plasmids 30174 and 30182, respectively), resulting in *msp12*-driven expression of the Wasabi or tdTomato fluorescent proteins, respectively. Mycobacteria were grown at 33 °C in Middlebrook 7H9 broth or on 7H10 agar (both by Difco) supplemented with 0.5% bovine serum albumin, 0.005% oleic acid, 0.2% glucose, 0.2% glycerol, 0.085% sodium chloride and 0.05% Tween-80 (broth culture only). 50 μg ml^{-1} hygromycin was added as appropriate. For sucrose counter-selection, 7H10 agar was supplemented with 10% sucrose. Single-cell suspensions of bacteria were prepared as described[32]. To prepare heat-killed crushed *M. marinum*, bacteria were incubated at 80 °C for 20 min and then homogenized in a Biospec Bead Beater together with 0.1 mm silica spheres for 1 min. The *P. aeruginosa* PAO1 fluorescent strain used in this study has been described[33]. The *S. aureus* Newman strain expressing pOS1-SdrC-mCherry #391 was a gift from J. Bubeck Wardenburg.

Targeted deletion of *mmpL7* and *pks15*. A 2,638 bp PstI fragment containing part of the *mmpL7* (MMAR_1764) open reading frame (ORF) was cloned into a pBluescript-derived vector, pBSXKpn.2 (C.L.C., unpublished observations). A 1,124 bp KpnI fragment internal to *mmpL7* was then excised and replaced with the *aph* cassette, conferring kanamycin resistance. The sucrose counter-selectable marker, *sacB*, and an additional marker, *hygA*, conferring hygromycin resistance, were then added to create pJENK7.1::Hyg. This construct was transformed into the wild-type reference strain, M, and kanamycin-resistant colonies were selected. Subsequent screening for sucrose sensitivity identified merodiploids that were verified by Southern blotting. One such merodiploid was then grown in liquid culture for 10 days and plated on sucrose-containing medium. Sucrose- and kanamycin-resistant hygromycin-sensitive colonies were then verified by Southern blotting to identify the *ΔmmpL7* mutant, KT15. This strain was verified to be deficient in surface localization of PDIM (data not shown), and exhibited colony morphology defects previously reported for *M. marinum* PDIM mutants[34]. The *pks15* (MMAR_1762) locus was deleted as follows. Flanking regions upstream and downstream of *pks15* were amplified by PCR using primers 5′pks15F (5′-CCGCTCG AGGGTGCGATGCGTGGTATC-3′), 5′pks15R.2 and (5′-CGACTAGTTCAGT TGCTCCTGTTCATG-3′), 3′pks15F, and (5′-GGAGCAACTGAACTAGTACC ATCCGACACCGACTG-3′) and 3′pks15R.2 (5′-CCGTCTAGAGTGGTGCTG TTCGGCGTC-3′), respectively. These fragments were sequentially inserted, directly adjacent to each other, into pBluescriptSK+::SacBHyg.1 (C.L.C., unpublished observations), a pBluescript derivative which contains *sacB* and *hygA* external to the multiple cloning site. The resulting construct, pPKS15KO, bears an unmarked deletion of the *pks15* ORF, and was used to transform strain M, and hygromycin-resistant colonies were selected. Putative merodiploids were verified by Southern blotting and then counter-selected on sucrose as described earlier, to produce the sucrose-resistant hygromycin-sensitive isolate (KT21), which was then verified by Southern blotting. Additional verification by thin-layer chromatography determined that PGL was absent, whereas PDIM production was retained (data not shown), consistent with deletion of *pks15* in *M. tuberculosis*[5].

Zebrafish husbandry and infections. Wild-type AB zebrafish were maintained as described[35]. Larvae (of undetermined sex given the early developmental stages used) were infected at 36–48 h post-fertilization (hpf) via caudal vein or HBV injection using thawed single-cell suspensions of known titre[32,35]. The number of animals to be used for each experiment was guided by past results with other bacterial mutants and/or zebrafish morphants. Larvae were randomly allotted to the different experimental conditions. Zebrafish husbandry and all experiments performed on them were in compliance with Institutional Animal Care and Use Committee approved protocols.

Microscopy and image-based quantification of infection level. Wide-field microscopy was performed using a Nikon Eclipse Ti-E equipped with a C-HGFIE 130W mercury light source, Chroma FITC (41001) filter, and ×2/0.10 Plan Apochromat objective. Fluorescence images were captured with a CoolSNAP HQ2 Monochrome Camera (Photometrics) using NIS-Elements (version 3.22). Quantification of fluorescent *M. marinum* infection using images of individual embryos using Fluorescent Pixel Count (FPC) was performed as previously described[32]. For confocal imaging, larvae were imbedded in 1.5% agarose (low melting point)[36]. A series of z-stack images with a 2 μm step size was generated through the infected HBV, using the galvo scanner (laser scanner) of the Nikon A1 confocal microscope with a ×20 Plan Apo 0.75 NA objective. Bacterial burdens were determined by using the three-dimensional surface-rendering feature of Imaris (Bitplane Scientific Software)[8].

Hindbrain assays. Macrophage recruitment assays were performed as previously described[35]. For determination of HBV infection burdens, 1 and 3 dpi larvae were mounted in 1.5% agarose and confocal z-stacks of 2 μm were obtained.

iNOS staining. Antibody staining of larvae was performed as described[8,37]. Larvae were then imaged using confocal microscopy and the number of infected macrophages that were positive for iNOS staining was determined for each larva.

iNOS scavengers. Fish were treated as previously described[38]. CPTIO or L-NAME (Sigma) were used at a final concentration of 500 μM and 1 mM, respectively, in 0.1% dimethylsulphoxide in fish water. Fish were incubated immediately following infection and fresh inhibitor was added every 24 h until bacterial burden was determined.

Morpholinos. The morpholinos described in Supplementary Table 1 were injected at the 1–4-cell stage as previously described[16].

Reverse transcription PCR to verify efficacy of MyD88 morpholino. RNA was extracted from pools of 15–40 embryos using TRIzol reagent (Life Technologies), treated with Turbo DNA-Free Kit (Life Technologies) and cDNA synthesized with PrimeScript (Takara). Primers used for PCR were as follows: actin, forward, 5′-ACCTGACAGACTACCTGATG, reverse, 5′-TGAAGGTGGTCTCATGGATAC; *myd88*, forward, 5′-ATGGCATCAAAGTTAAGTATAGACC, reverse, 5′-AGG GCAGTGAGAGTGCTTTG.

Identification of candidate CCR2 orthologue in zebrafish. Basic Local Alignment Search Tool (BLAST) searches of the zebrafish genome (http://www.ensembl.org) identified two closely related *CCR*-like genes on chromosome 16: ENSDARG00000079829 and ENSDARG00000062999. In BLAST comparisons to the human genome, ENSDARG00000079829 was found to have the highest homology to human CCR2 (*E* value 8.8×10^{-112}), whereas ENSDARG00000062999 was most highly homologous to human CCR4 (*E* value 2×10^{-90}). In addition, annotation of the zebrafish genome from NCBI annotates ENSDARG00000079829 as a *CCR2*-like gene. We confirmed expression of the mRNA and identified the short 5′ upstream exon ATGTCGGCGACACAAAACAGTA using 5′ rapid amplification of cDNA ends (RACE)[39].

Identification of zebrafish CCL2 orthologue. Protein sequences of human and mouse CCL2 were used to interrogate the zebrafish genome by BLAST. Expression levels of the four most closely related zebrafish proteins were then examined at 3 hpi to identify the likely functional orthologue (Extended Data Fig. 9a). Of the four candidates, only ENSDARG00000041835 was significantly induced at 3 hpi. Knockdown of ENSDARG00000041835 resulted in a decrease in macrophage recruitment into the HBV at 3 hpi (Extended Data Fig. 9b).

Quantitative real-time PCR. cDNA was synthesized from pools of 20–40 larvae as previously described[37]. Quantification of *ccl2* RNA levels was determined using SYBR green and the following primer pair: 5′-GTCTGGTGCTCTTCGCTTTC-3′ and 5′-TGCAGAGAAGATGCGTCGTA-3′.

Infectivity assay. 2 dpf larvae were infected via the HBV[35] with an average of 0.8 bacteria per injection. Fish harbouring 1–3 bacteria were then identified at 5 hpi by confocal microscopy. These infected fish were then evaluated at 5 dpi and were scored as infected or uninfected, based on the presence or absence of fluorescent bacteria.

Mice, aerosol infections, and flow cytometry. C57BL/6 mice were purchased from Jackson Laboratories. All mice were housed under specific pathogen-free conditions at the Seattle Biomedical Research Institute, and all experiments were performed in compliance with the respective Institutional Animal Care and Use Committee approved protocols. Ten-week-old female mice were randomized to the different experimental groups. The number of mice to be used to adequately power the experiment was guided by the results of the corresponding zebrafish experiments. A stock of *M. tuberculosis* strain H37Rv or the isogenic PDIM-deficient *ΔdrrA* strain was sonicated before use and mice were infected in an aerosol infection chamber (Glas-Col) with approximately 200 c.f.u. of H37Rv or 1,000 c.f.u. of *ΔdrrA* to achieve similar bacterial burdens at 21 dpi. The infectious dose in each experiment was determined by plating lung tissue of two mice from each group. Colonies on 7H10 agar plates were counted after 21 days of incubation at 37 °C. Lung tissue was perfused with 5 ml of PBS administered through the right ventricle of the heart, finely chopped using a gentleMACS Octo Dissociator (Miltenyi Biotec) and incubated at 37 °C for 30 min in HEPES buffer containing Liberase Blendzyme 3 (Roche Applied Science). After digestion, single-cell suspensions were prepared by passing tissue through a cell strainer. Single-cell suspensions were then stained for flow cytometric analysis. Lung single-cell suspensions were surface stained at 4 °C for 20 min in the presence of Fc block (24G2) with the following antibodies from eBioscience: PE-Cy7-labelled anti-CD4 (GK1.5, eBioscience), anti-CD8α (53-6.7, eBioscience), anti-CD11c (N418), and FITC-labelled anti-Ly6G (1A8) to exclude T cells, dendritic cells and neutrophils. Alveolar macrophages were excluded based on their high CD11c expression and autofluorescence. PerCPCy5.5-labelled anti-Ly6C (HK1.4) and APC-efluor-780-labelled anti-CD11b (M1/70) were used to identify CD11b^{+}Ly6C^{hi} monocytes. Intracellular staining was done after fixation and permeabilization, following the manufacturer's recommendations (eBioscience). Cells were fixed and permeabilized using eBioscience's Fix/Perm buffer for 1 h at 4 °C, followed by staining for iNOS with anti-NOS2 Alexa Fluor 405 (C-11, Santa Cruz Biotechnology) or mouse IgG1 isotype control

for 30 min at 4 °C. Samples were analysed on an LSR-II (BD Biosciences) and FlowJo Software (Treestar).

Statistics. Statistical analyses were performed using Prism 5.01 (GraphPad). For data sets requiring $\log_{10}$ transformation before ANOVA, embryos with no detectable fluorescence above background were assigned a value of 0.9, with 1 being the limit of detection, before $\log_{10}$ transformation. Post-test P values are as follows: $*P < 0.05$; $**P < 0.01$; $***P < 0.001$.

31. Cosma, C. L., Klein, K., Kim, R., Beery, D. & Ramakrishnan, L. *Mycobacterium marinum* Erp is a virulence determinant required for cell wall integrity and ntracellular survival. *Infect. Immun.* **74,** 3125–3133 (2006).
32. Takaki, K., Cosma, C. L., Troll, M. A. & Ramakrishnan, L. An *in vivo* platform for rapid high-throughput antitubercular drug discovery. *Cell Rep.* **2,** 175–184 (2012).
33. Brannon, M. K. *et al. Pseudomonas aeruginosa* Type III secretion system interacts with phagocytes to modulate systemic infection of zebrafish embryos. *Cell. Microbiol.* **11,** 755–768 (2009).
34. Yu, J. *et al.* Both phthiocerol dimycocerosates and phenolic glycolipids are required for virulence of *Mycobacterium marinum*. *Infect. Immun.* **80,** 1381–1389 (2012).
35. Takaki, K., Davis, J. M., Winglee, K. & Ramakrishnan, L. Evaluation of the pathogenesis and treatment of *Mycobacterium marinum* infection in zebrafish. *Nature Protocols* **8,** 1114–1124 (2013).
36. Davis, J. M. & Ramakrishnan, L. The role of the granuloma in expansion and dissemination of early tuberculous infection. *Cell* **136,** 37–49 (2009).
37. Clay, H. *et al.* Dichotomous role of the macrophage in early *Mycobacterium marinum* infection of the zebrafish. *Cell Host Microbe* **2,** 29–39 (2007).
38. Lepiller, S. *et al.* Imaging of nitric oxide in a living vertebrate using a diaminofluorescein probe. *Free Radic. Biol. Med.* **43,** 619–627 (2007).
39. Maruyama, I. N., Rakow, T. L. & Maruyama, H. I. cRACE: a simple method for identification of the 5′ end of mRNAs. *Nucleic Acids Res.* **23,** 3796–3797 (1995).

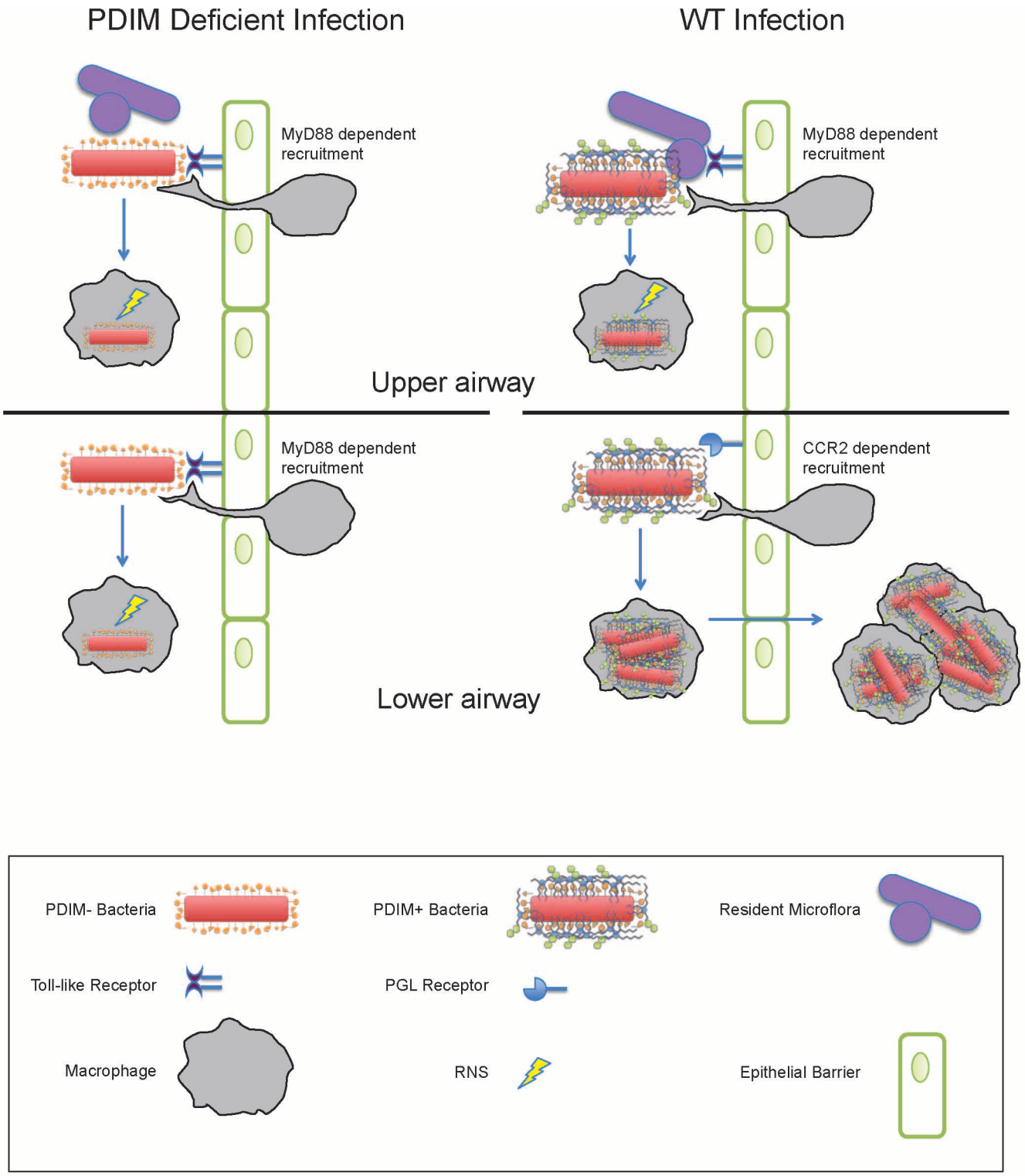

Extended Data Figure 1 | Coordinate use of PDIM-mediated immune evasion and PGL-mediated recruitment by pathogenic mycobacteria. Models for infection with wild-type (WT) and PDIM-deficient mycobacteria are shown in the context of the relatively sterile lower airway versus the upper airway, with its higher levels of resident microflora and inhaled environmental organisms.

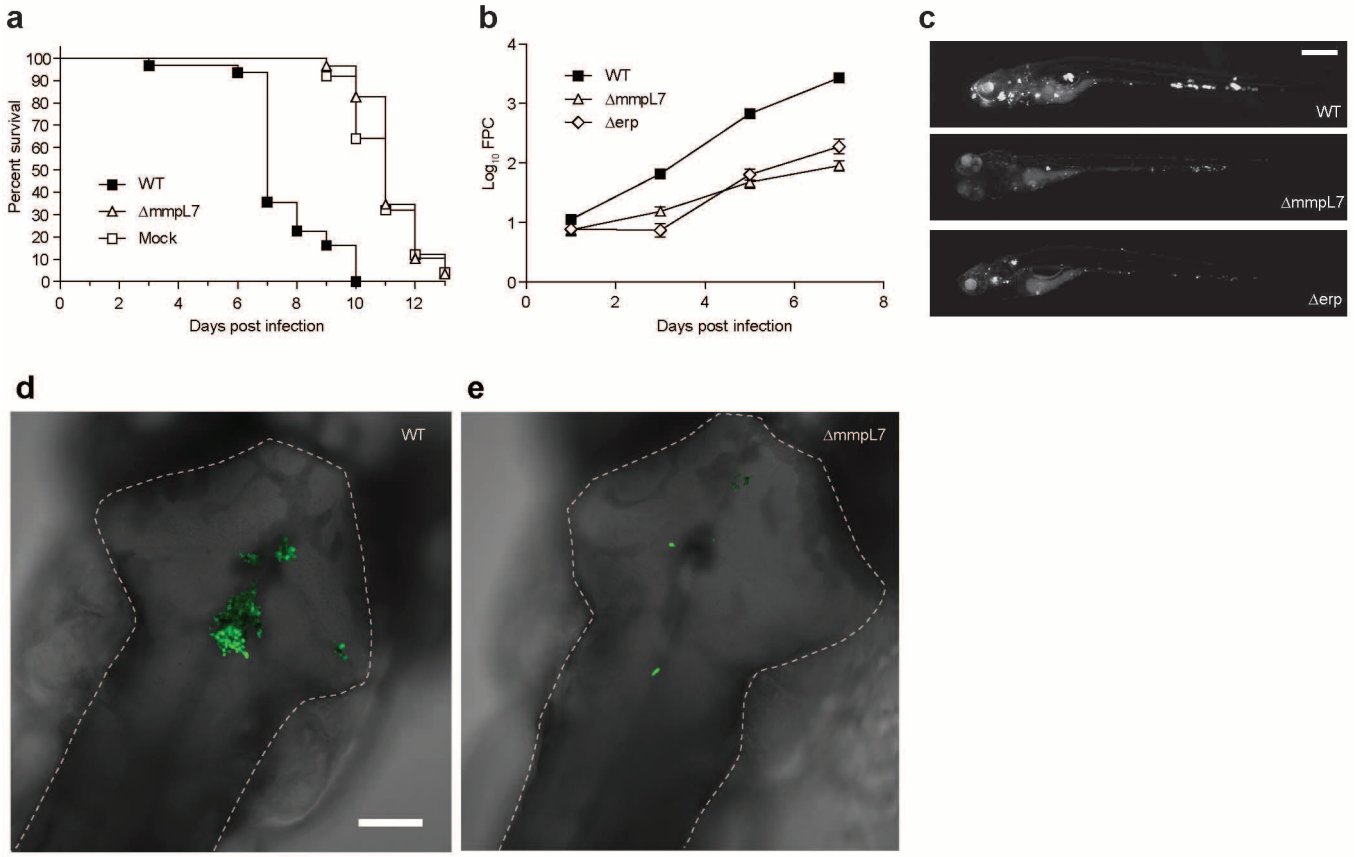

Extended Data Figure 2 | *ΔmmpL7* bacteria are attenuated in zebrafish larvae. **a**, Kaplan–Meier graph showing daily survival of larvae infected via caudal vein injection with medium (mock), 29 wild-type or 70 Δ*mmpL7* *M. marinum*. $N = 25$ (mock), 31 (wild-type), or 29 (Δ*mmpL7*) larvae per group. Mean time to death (days): mock (11), wild type (7.6) and Δ*mmpL7* (11.2). Survival was compared by log-rank test: wild type versus mock and wild type versus Δ*mmpL7*, $P < 0.0001$; mock versus Δ*mmpL7*, $P = 0.5601$. **b**, **c**, Larvae were infected via caudal vein injection 1 dpf with 550 wild-type, 650 *ΔmmpL7*, or 700*Δerp*, fluorescent *M. marinum*. **b**, Infection burdens were measured by Fluorescent Pixel Count (FPC; mean ± s.e.m.). **c**, Representative images at 7 dpi. $N = 29$ (wild-type and Δ*mmpL7*) or 30 (Δ*erp*) larvae per group. Scale bar, 500 μm. At 3, 5 and 7 dpi, $\log_{10}$ FPC was compared by ANOVA, with Dunnett's post-test. ***$P < 0.001$. **d**, **e**, Representative images from wild-type (**d**) and Δ*mmpL7* (**e**) *M. marinum* HBV infections quantified in Fig. 1d. $N = 18$ (wild-type) or 16 (Δ*mmpL7*) larvae per group. HBVs are outlined with a dashed white line. Scale bar, 100 μm.

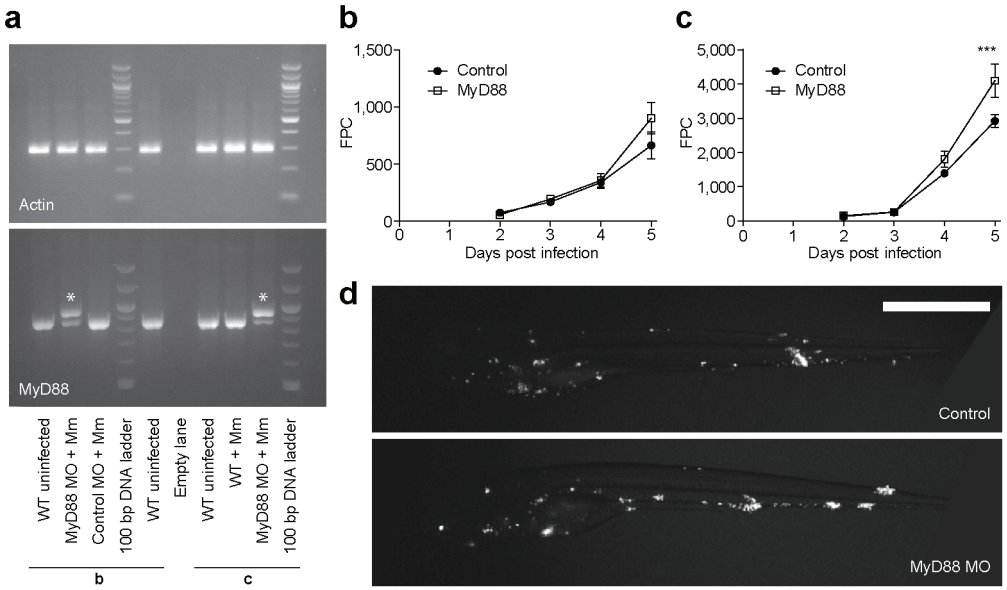

Extended Data Figure 3 | Knockdown of MyD88 results in a late, dose-dependent hypersusceptibility to *M. marinum* systemic infection. **a**, RT–PCR for actin (top) and *myd88* (bottom), demonstrating that that the majority of *myd88* transcripts at 7 dpf are abnormal in MyD88 morphants. Lanes marked '**b**' and '**c**' correspond to morphants from the same experiments depicted in panels **b** and **c**, respectively. The abnormal larger transcript (indicated by an asterisk) results from the inclusion of intron 2 in the final transcript, incorporating a premature stop codon that truncates the protein before the TIR (Toll/interleukin receptor) domain. **b**, **c**, Caudal vein infection of MyD88 morphants with 141 (**b**) or 325 (**c**) c.f.u. *M. marinum*/larva. Bacterial burden was assessed by FPC, values plotted represent the mean ± s.e.m. Time points were compared by one-way ANOVA and Bonferroni's post-tests. *** $P < 0.001$. **d**, Representative images of larvae at 5 dpi from experiment in **c**, $N = 30$ control, 15 MyD88 morphant. Scale bar, 500 μm.

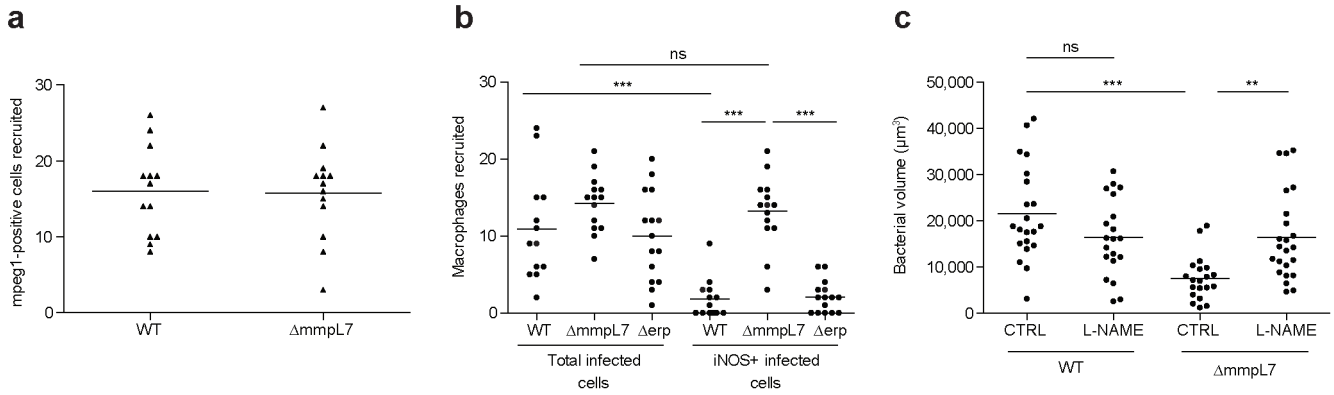

Extended Data Figure 4 | Characteristics of macrophages recruited to wild-type and PDIM-deficient bacteria. **a**, Mean Mpeg1-positive macrophages recruited at 3 hpi into the HBV of wild-type fish after infection with 80 wild-type or Δ*mmpL7 M. marinum*. **b**, Data from Fig. 2c expressed as mean numbers of total infected macrophages and iNOS-expressing infected macrophages after HBV infection with 80 wild-type, Δ*mmpL7*, or Δ*erp M. marinum*. **c**, Bacterial burdens after L-NAME treatment. Mean bacterial burdens of 2 dpf control (CTRL)- or iNOS inhibitor (L-NAME)-treated fish after HBV infection with 80 wild-type or Δ*mmpL7 M. marinum*. NS, not significant.

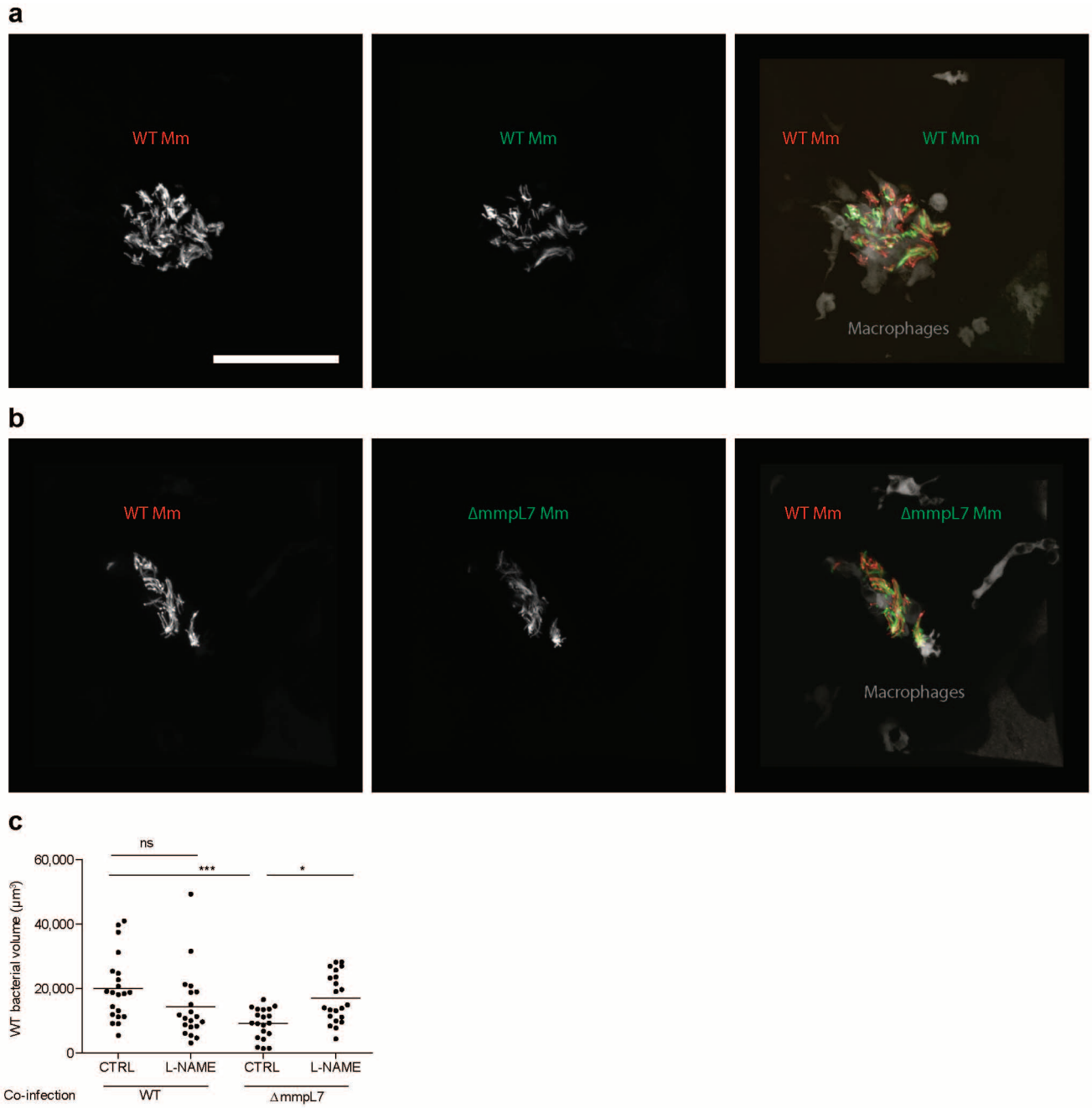

Extended Data Figure 5 | Wild-type bacterial burdens after co-infection with wild-type or Δ*mmpL7* bacteria. Representative images from the HBV co-infections quantified in Fig. 2e. **a**, **b**, Red fluorescent wild-type (WT) *M. marinum* co-infected with green fluorescent wild-type (**a**) or Δ*mmpL7* (**b**) *M. marinum*. $N = 18$ (wild-type) and 19 (Δ*mmpL7*) larvae per group. Scale bar, 50 µm. **c**, Wild-type bacterial burdens after co-infection with wild-type or Δ*mmpL7 M. marinum* with and without L-NAME treatment. Significance tested by one-way ANOVA with Bonferroni's post-test for comparisons shown.

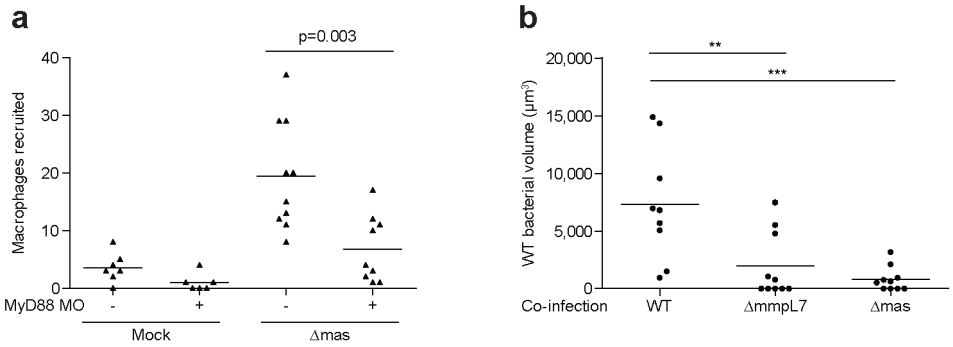

Extended Data Figure 6 | MyD88-dependent macrophage recruitment occurs in response to PDIM deficiency rather than being due to loss of another MmpL7-exported product. a, Mean macrophage recruitment at 3 hpi into the HBV of wild-type or MyD88-morphant (MO) larvae after infection with 80 Δ*mas M. marinum*. Student's unpaired *t*-test. **b**, Mean surviving bacterial volume of red fluorescent wild-type *M. marinum* (initial infection dose of 30–40 c.f.u.) when co-infected with 30–40 green fluorescent wild-type, Δ*mmpL7* or Δ*mas M. marinum* at 3 dpi. Representative of two separate experiments. Significance tested by one-way ANOVA with Tukey's post-test.

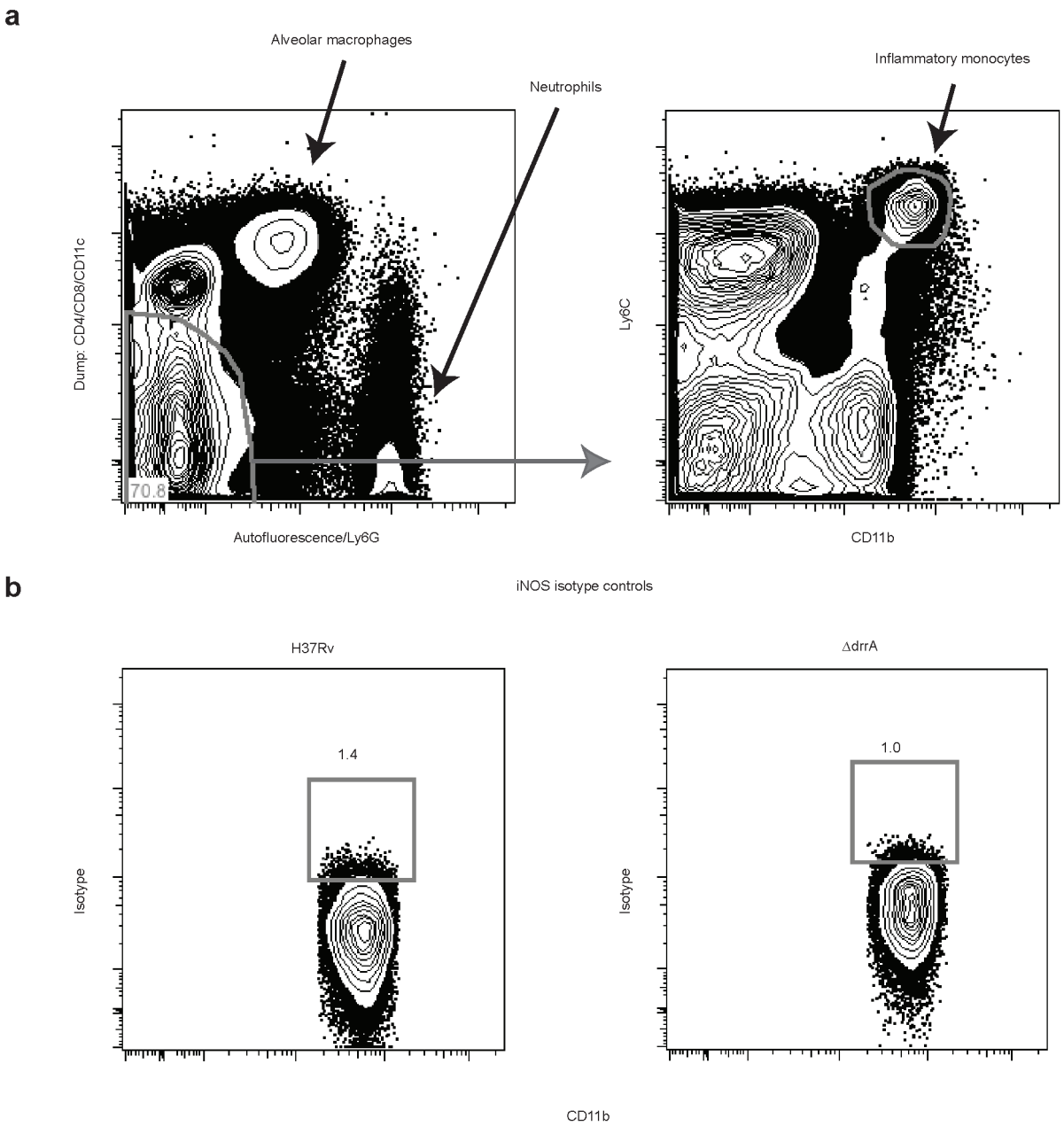

Extended Data Figure 7 | Gating strategy and isotype controls for iNOS staining of mouse lung. **a**, Representative gating strategy for isolation of inflammatory monocytes. A dump channel containing anti-CD4, CD8 and CD11c was plotted against a channel exhibiting autofluorescence and also containing anti-Ly6G. Using these markers, T cell, dendritic cell, alveolar macrophage, and neutrophil cell populations were excluded from the double-negative gate. Inflammatory monocytes were identified within the double-negative population by their co-expression of Ly6C and CD11b. These cells were then evaluated for intracellular iNOS expression. **a**, $N = 4$ per group (Fig. 3a, b) or **b**, with isotype control antibodies, $N = 4$ per group.

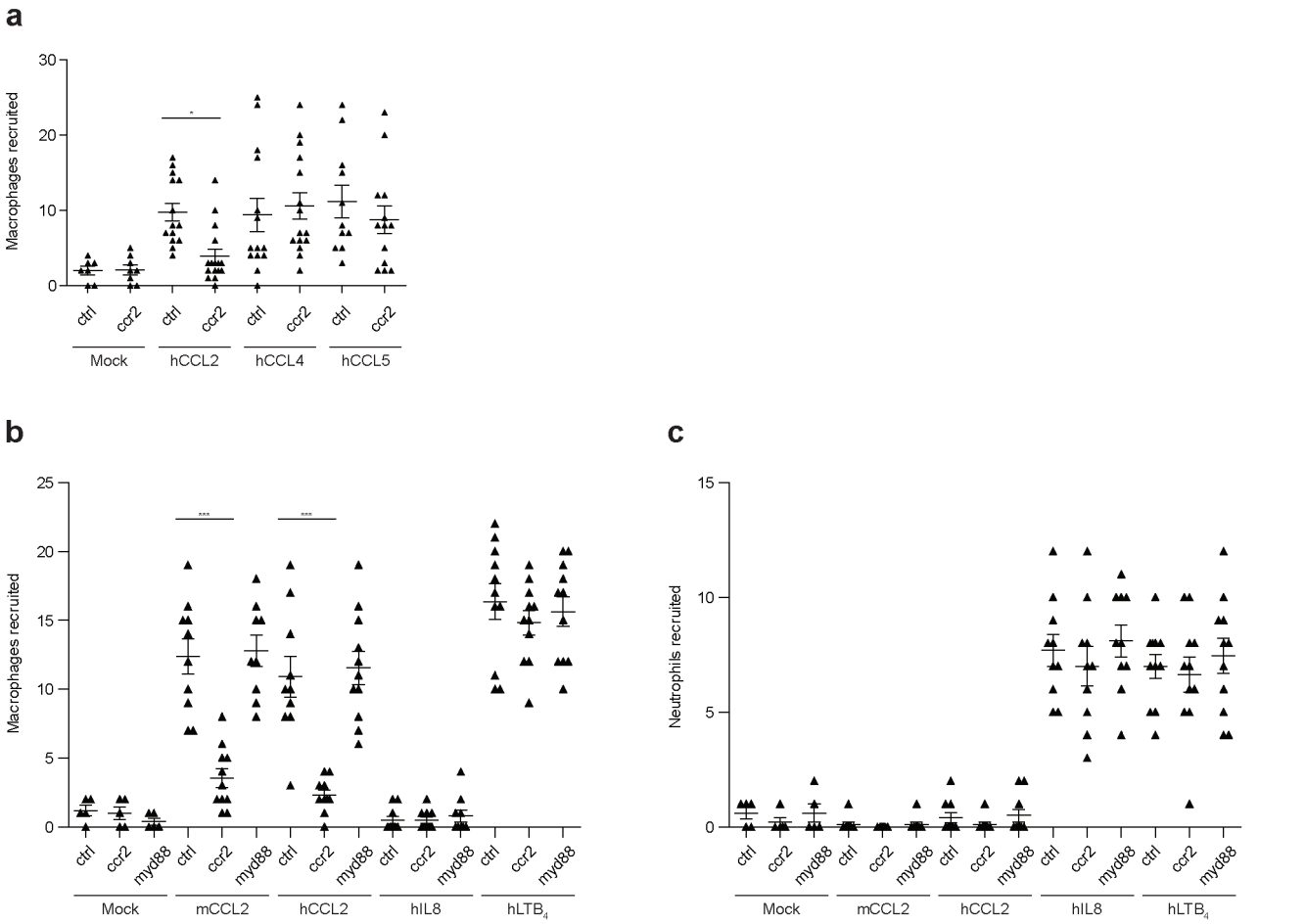

Extended Data Figure 8 | Specificity of CCL2-mediated macrophage recruitment in wild-type and CCR2-morphant larvae **a**, Mean macrophage recruitment at 3 hpi into the HBV of control (ctrl), or CCR2-morphant (CCR2) larvae after injection of vehicle control ('mock'; 0.1% BSA in PBS), human CCL2 (hCCL2), human CCL4 (hCCL4), or human CCL5 (hCCL5). **b**, **c**, Mean macrophage (**b**) and neutrophil (**c**) recruitment at 3 hpi into the HBV of control (CTRL), CCR2-morphant (CCR2), or MyD88-morphant (MyD88) larvae after injection of vehicle control (mock), murine CCL2 (mCCL2), human CCL2 (hCCL2), human IL-8 (hIL-8), or human LTB4 (hLTB4). Representative of three separate experiments. Significance assessed by one-way ANOVA with Bonferroni's post-test for the comparisons shown. $*P < 0.05$; $***P < 0.001$.

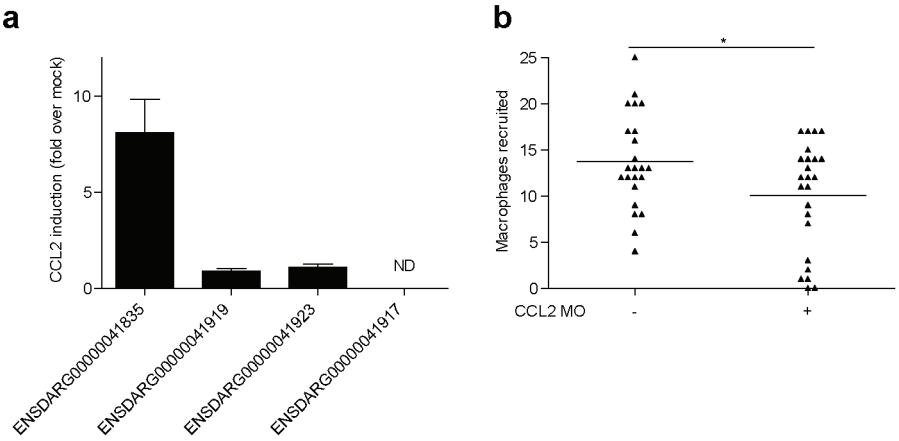

Extended Data Figure 9 | Identification of zebrafish CCL2 orthologue. **a**, mRNA levels of potential CCL2 orthologues (mean ± s.e.m. of four biological replicates) induced at 3 h after caudal vein infection of 2 dpf larvae with 250–300 wild-type *M. marinum*. These assays were performed on the same cDNA pools as the data presented in Fig. 4b. **b**, Mean macrophage recruitment at 3 hpi into the HBV of wild-type or CCL2 morphant (MO) fish following infection with 80 *M. marinum*. Representative of two separate experiments.

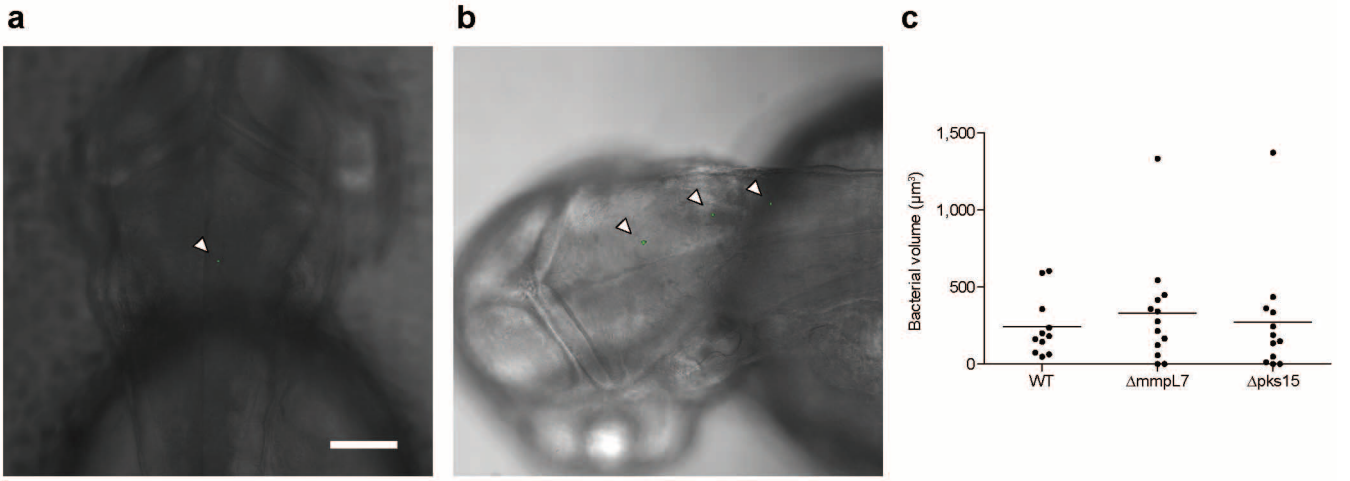

Extended Data Figure 10 | Infectivity assay. **a**, **b**, Representative 5 hpi images from Fig. 4d following HBV infection with one (**a**) or three (**b**) *M. marinum*. Scale bar, 100 µm. *N* values for fish represented in **a** and **b** (that is, those found to be infected with 1–3 bacteria) are presented in Fig. 4d (18, 22, 28, 28, 28, 28, 22, 22 for the respective conditions as specified in the figure). **c**, Mean bacterial burdens 5 h after HBV infection with 1–3 wild-type (WT), Δ*mmpL7* or Δ*pks15 M. marinum*.